Mechanical and electromechanical coupling in carbon nanotube distortions

Yu. N. Gartstein,[1] A. A. Zakhidov,[1,2] and R. H. Baughman,[3,2]
[1]*Department of Physics, University of Texas at Dallas, Richardson, Texas 75083, USA*
[2]*UTD-NanoTech Institute, University of Texas at Dallas, Richardson, Texas 75083, USA*
[3]*Department of Chemistry, University of Texas at Dallas, Richardson, Texas 75083, USA*
(Received 15 May 2003; published 16 September 2003)

A simple approach is presented for using bond-stretching and bond-bending modes to describe the static deformations of carbon nanotubes and related actuation effects. This approach allows us to analyze various phenomena in a unified way and to clarify their relationships. We discuss gap energy modulation by external strains, dimensional and torsional deformations caused by charge injection, and stretch-induced torsion. We show how symmetry determines the property dependence on the chiral angle of nanotubes. Electrically driven actuator responses related to deformation-induced modulation of electron kinetic energy are particularly interesting and relevant for applications. The strong oscillatory dependence of these responses on the nanotube geometry is explained within an intuitively clear picture of bonding patterns. We show how anisotropic (shear) deformations play an important role in nanotubes, making their responses distinctly different from graphite's.

DOI: 10.1103/PhysRevB.68.115415 PACS number(s): 61.46.+w, 73.22.−f, 71.38.−k, 85.85.+j

I. INTRODUCTION

Carbon nanotubes are particularly noteworthy nanoscopic systems[1] whose widely investigated electronic and mechanical properties are interesting for diverse applications.[2,3] In this paper we study how microscopic atomic displacements within nanotubes provide for specific mechanical and electromechanical couplings, which are important to interconvert electrical and mechanical energy and could be used in nanoscale (electro)mechanical devices.[4,5] We describe the deformations of nanotubes resulting from the charge injection as well as coupling between stretching and torsional deformations.

Electromechanical actuation using single-wall nanotubes (SWNTs) has been demonstrated in electrochemical cells.[6] Actuator strains of above 1% have been observed,[3] which is about ten times that of high modulus ferroelectrics, suggesting the technological opportunity for direct conversion of electrical energy into mechanical energy. Currently available nanotube sheets and long fibers comprise bundles of SWNTs. Each bundle typically contains from 30 to 100 SWNTs of various diameters and chiral vectors (N,M):[1] from zigzag $(N,0)$ to armchair (N,N) tubes. In a recent publication[7] we studied a simplified electron-lattice model at low charge injection levels and showed that the electromechanical actuation of SWNTs strongly depends on (N,M). We found that the electromechanical response of individual tubes, particularly semiconducting zigzag nanotubes, can be much larger than for graphite. Here we extend this study using a more complete picture of elastic interactions and including torsional deformations. We also provide a simple bonding picture to explain the behavior of different nanotube types.

Stretch-induced torsion of SWNTs has been found in molecular dynamics simulations.[8] Here we show that this effect is caused by curvature-derived elastic anisotropy and that the maximum stretch-induced torsion is expected for nanotubes having a chiral angle midway between that for armchair and zigzag tubes. The predicted stretch-induced torsional rotations are small unless the carbon nanotubes are quite long. We show that nanotubes with inherent elastic anisotropy, such as BC_2N tubes,[9] can exhibit increased stretch-induced torsional rotations.

Our focus will be on providing a simple, unified description of the relationships between various effects. The approach consists of finding the static lattice distortion patterns **D** that minimize the total per-carbon adiabatic energy of the system:

$$E(\mathbf{D}) = U(\mathbf{D}) + E_{\mathrm{el}}(\mathbf{D}), \tag{1}$$

where U is the lattice elastic potential energy, including energies of all valence electrons of the *undoped* system, and E_{el} is the energy of δn *extra* electrons per carbon that can be added.

We find it convenient to discuss static distortions of nanotubes in terms of effective 2-*d* displacements of atoms of a parent graphene sheet out of which nanotubes are rolled.[1] Bond-stretching and bond-bending displacements of the hexagonal atomic lattice are considered that can form both *isotropic* and *anisotropic* distortion modes. The latter modes turn out to be responsible for many interesting effects specific to nanotubes. Appropriate empirical expressions for U will be built that are based entirely on the symmetry requirements, in the spirit of the continuum mechanics, and connections being established between the microscopic displacements picture and the macroscopically observable distortions (Sec. II). For E_{el} we use a tight-binding model of π-electron bands[1] whose parameters can be affected by the lattice distortions (Sec. III). When a strain is applied to the undoped system, the deformation **D** occurs so as to minimize U and this results in modulation of some electronic parameters, such as the gap energy[10] (Sec. IV), and, possibly, in a strain ''along another direction'' (Sec. VI). Conversely, if charges are added to the system, the lattice will try to accommodate them with the deformation **D** that minimizes E (Sec. V). For

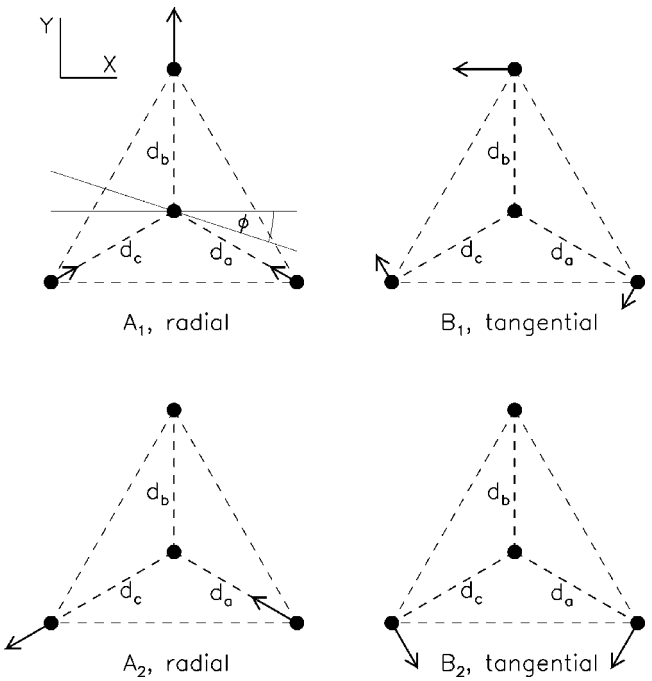

FIG. 1. Four carbon atoms of the repeating motif are depicted along with the three types of bonds d_a, d_b, and d_c. The carbon atom displacements corresponding to the defined anisotropic distortion modes are schematically shown in the four panels. The nanotube axis is at the angle ϕ to the x axis.

illustrative purposes, some parametrization will be used to carry out numerical calculations.

II. MACROSCOPIC AND MICROSCOPIC 2-*d* DISTORTIONS

Elastic in-plane deformations of the graphene sheet provide a natural basis for the effective 2-*d* description of nanotube deformations. An arbitrary 2-*d* crystal structure may have many atoms in the unit cell (graphene has two atoms) and, correspondingly, many deformation degrees of freedom. From the standpoint of *uniform* macroscopic distortions, however, ''internal'' degrees of freedom are disguised and the only static observable is the deformation of the unit cell as a whole or, alternatively, of the triangle built of the primitive lattice vectors and assumed periodically repeated. To specify the 2-*d deformation* of the triangle, one needs three parameters, precisely as many as is needed to specify the uniform in-plane deformations of a 2-*d* elastic continuum. Let us choose a convenient 2-*d* system of coordinates with axes x and y (axes in Fig. 1 are related to the underlying hexagon structure). With overall translation and rotation excluded, a general linear (uniform) deformation [displacement $(\delta x, \delta y)$ of the point (x,y)] of the elastic continuum can be described as

$$\begin{pmatrix} \delta x \\ \delta y \end{pmatrix} = \begin{pmatrix} \gamma_0 + \gamma_x & \eta_x \\ \eta_x & \gamma_0 - \gamma_x \end{pmatrix} \begin{pmatrix} x \\ y \end{pmatrix}. \tag{2}$$

Parameter γ_0 corresponds to isotropic distortions, while parameters γ_x and η_x correspond to anisotropic distortions and are components of the pure shear strain tensor.

In nanotubes, there would also be another natural system of coordinates related to the nanotube axis (in Fig. 1 the x axis is at angle $\phi > 0$ to the nanotube axis). With the coordinates rotated as

$$\begin{pmatrix} x_1 \\ y_1 \end{pmatrix} = \begin{pmatrix} \cos\phi & -\sin\phi \\ \sin\phi & \cos\phi \end{pmatrix} \begin{pmatrix} x \\ y \end{pmatrix}, \tag{3}$$

γ_0 remains invariant while shear components are known to transform as

$$\begin{pmatrix} \gamma \\ \eta \end{pmatrix} = \begin{pmatrix} \cos 2\phi & -\sin 2\phi \\ \sin 2\phi & \cos 2\phi \end{pmatrix} \begin{pmatrix} \gamma_x \\ \eta_x \end{pmatrix}.$$

Macroscopic deformations of the tube as a whole are defined and measured with respect to the tube axis. The three parameters (γ_0, γ, η) translate into the observable longitudinal dimensional change $\delta L/L = \gamma_\parallel = \gamma_0 + \gamma$, the transverse change $\delta R/R = \gamma_\perp = \gamma_0 - \gamma$, and the torsional deformation $\delta\phi_l = \eta/\pi R$ (the latter is in turns per unit length, R being the tube radius).

For a full description of the 2-*d* deformation of the graphene unit cell with two atoms, one however needs five parameters. We consider the deformations in terms of radial (bond-stretching: δ_a, δ_b, δ_c for, respectively, bonds d_a, d_b, d_c) and tangential (bond-bending: r_a, r_b, r_c) displacements of carbon atoms, as should be clear from Fig. 1. Let us express those displacements as linear combinations of the corresponding *isotropic* $(S,\ Q)$ and *anisotropic* $(A_1,\ A_2)$ and $(B_1,\ B_2)$ distortion modes, e.g.,

$$\begin{aligned} \delta_a &= S/3 - A_1/2\sqrt{3} - A_2/2, \\ \delta_b &= S/3 + A_1/\sqrt{3}, \\ \delta_c &= S/3 - A_1/2\sqrt{3} + A_2/2 \end{aligned} \tag{4}$$

for radial displacements and similarly for r_a, r_b, and r_c through Q, B_1, and B_2. It is clear, however, that the Q mode is not a deformation mode; it describes the overall rotation of the triangle, which is irrelevant for our purposes. Similarly to the exclusion of the translations out of consideration, we set $Q=0$ in agreement with the definition (2) [nonzero Q would in general require two different off-diagonal elements of the transformation matrix in Eq. (2)]. The five modes left can be used as five convenient necessary parameters. The isotropic mode S describes the overall size change of the triangle. The anisotropic distortions A_i and B_i result in the triangle shape modifications indicated in Fig. 1. It is also useful to introduce the rotated anisotropic deformation modes $(A_\parallel,\ A_\perp)$ and $(B_\parallel,\ B_\perp)$ defined with respect to the nanotube axis. They respectively relate to $(A_1,\ A_2)$ and $(B_1,\ B_2)$ as (x_1, y_1) to (x,y) in Eq. (3).

From Fig. 1 and from the corresponding definitions, one can obtain the following compact expressions for the macroscopic deformations:

$$d\cdot\gamma_0 = S/3,$$

$$d\cdot\gamma = (B-A)/2\sqrt{3}, \tag{5}$$

$$d\cdot\eta = (C-D)/2\sqrt{3},$$

where

$$A = A_\parallel \cos 3\phi + A_\perp \sin 3\phi,$$

$$B = B_\parallel \sin 3\phi - B_\perp \cos 3\phi,$$

$$C = -A_\parallel \sin 3\phi + A_\perp \cos 3\phi, \tag{6}$$

$$D = B_\parallel \cos 3\phi + B_\perp \sin 3\phi.$$

The length unit d above stands for the undeformed nearest neighbor carbon-carbon bond length, another length unit to be used is the second order carbon-carbon distance $a = d\sqrt{3}$. Notice that macroscopic results (5) and (6) are *invariant* with respect to rotation $\phi \to \phi + 2\pi/3$ as one should expect from the symmetry of the hexagon structure.

The elastic energy of the in-plane deformations of the graphene sheet is known to be invariant with respect to the rotation of the 2-d system of coordinates. Using all rotationally invariant combinations of the introduced deformation modes, the harmonic deformation energy per carbon atom can in general be written as

$$U^0 = \frac{K_S}{2}S^2 + \frac{K_A}{2}(A_\parallel^2 + A_\perp^2) + \frac{K_B}{2}(B_\parallel^2 + B_\perp^2) + K_{AB}(A_\parallel B_\perp - A_\perp B_\parallel). \tag{7}$$

It is up to *ab initio* and/or empirical models to establish numerical values of the elastic constants. In this paper, we will be using some estimates for illustrative purposes. For instance, a good representation of the elastic properties of graphene in an empirical force constant model is achieved by including terms up to four near neighbor levels as described and referenced in Ref. 1. Using this model, one can express the elastic constants in Eq. (7) through the force constants $\phi_i^{(j)}$, e.g.,

$$K_S = \phi_r^{(1)}/6 + \phi_r^{(2)} + 2\phi_r^{(3)}/3 + 7\phi_r^{(4)}/3$$

for the S mode, and so on. Then, using numerical values of the force constants quoted on p. 169 of Ref. 1, one would arrive at the following magnitudes of the elastic constants (in eV/Å^2):

$$K_S = 7.74,\ K_A = 4.56,\ K_B = 7.14,\ K_{AB} = 1.21. \tag{8}$$

With these numbers, A_i modes turn out to be softer than B_i modes, and the coupling between A_i and B_j modes is relatively weak. It is useful to compare relative strengths in Eq. (8) to the nearest neighbor elastic spring model used in Ref. 7 where $K_S = K/6$ and $K_A = K/4$: evidently (8) yields relatively softer A_i modes.

For a given macroscopic distortion (γ_0, γ, η) of the undoped sheet, the microscopic distortion modes adjust so as to minimize the microscopic energy (7). The resulting rotationally invariant *macroscopic* deformation energy per carbon is

$$U_{\rm m}^0 = \frac{C_0}{2}\gamma_0^2 + \frac{C_{\rm sh}}{2}(\gamma^2 + \eta^2), \tag{9}$$

where the effective elastic energies $C_0 = 9d^2K_S$ and $C_{\rm sh} = 12d^2 Z_{ab}/z_{ab}$.[11] While going from Eq. (7) to Eq. (9), one can also answer an interesting question: When are displacements of *all* atoms in the unit cell of graphene describable using a 2-d continuum? For this to happen, the optimal distortion modes should satisfy $A_\parallel = B_\perp$ and $A_\perp = -B_\parallel$, which requires that $K_A = K_B$. With the numbers in Eq. (8) and $d = 1.42$Å, the elastic energies are $C_0 = 140.5$ eV and $C_{\rm sh} = 81.1$ eV. The effective 2-d Poisson ratio $\nu = (C_0 - C_{\rm sh})/(C_0 + C_{\rm sh})$ turns out to be 0.27, close to the earlier reported[12] value within the same force constant model, and the in-plane stiffness per carbon is $C = C_0 C_{\rm sh}/(C_0 + C_{\rm sh}) = 51.4$ eV.

When the graphene sheet is wrapped to form a carbon nanotube, the effective 2-d elastic description would undergo certain changes. From the results of *ab initio* calculations,[13,14] it is known that even in the ground state of nanotubes the equilibrium bond lengths d_a, d_b, and d_c can differ from each other and are different from the graphene bond length d. These effects can easily be absorbed in our description by thinking that the ground states of nanotubes are somewhat deformed (with respect to graphene). It should be understood that the deformation is in general anisotropic (the rotational invariance is lifted since a new selected direction would now exist—the nanotube axis). Using general symmetry considerations,[15] one can show that the deformation of the ground state can be described by three R-dependent distortion parameters (S_R, A_R, B_R) so that

$$A_\parallel = A_R \cos 3\phi, \quad A_\perp = A_R \sin 3\phi,$$

$$B_\parallel = B_R \sin 3\phi, \quad B_\perp = -B_R \cos 3\phi. \tag{10}$$

Note that Eqs. (10) are required by the symmetry. That is, extraction of the functions (S_R, A_R, B_R) from *ab initio* data[13,14] for, say, armchair nanotubes would be sufficient to describe the deformed ground states for the tubes of arbitrary chirality. In this paper we do not pursue these numerical fits to the *ab initio* data.

When using expression (7) for the elastic energy, we now understand that the deformation modes $S, A_\parallel, \ldots$ used there are calculated relative to their values in the corresponding ground states. In addition to this, however, the curvature in nanotubes of a finite radius R also modifies the very elastic couplings. First, the elastic constants K in Eq. (7) can be renormalized with corrections $\propto 1/R^2 + \cdots$. That is, all coefficients in Eqs. (7) and (9) and quantities derived from them are in general R dependent. Second, the rotational invariance of the elastic energy is also lifted. Using the same symmetry considerations,[15] one can show that this axial symmetry breaking in the harmonic approximation will occur in the form $U = U^0 + \delta U$,

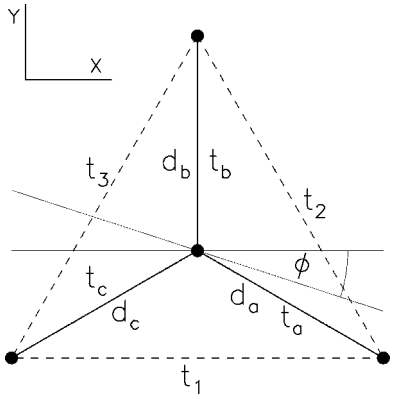

FIG. 2. NNH and SNH integrals, whose modulation is taken into account.

$$\delta U = K^a_{SA} SA + K^a_{SB} SB + \frac{K^a_A}{2}(A^2_\parallel - A^2_\perp) + \frac{K^a_B}{2}(B^2_\parallel - B^2_\perp) + K^a_{AB}(A_\parallel B_\perp + A_\perp B_\parallel), \quad (11)$$

where definitions (6) have been used and anisotropy parameters $K^a \propto 1/R^2 + \cdots$. While the isotropic deformation energy (7) is already sufficient for description of some of the effects, the elastic anisotropy expressed in Eq. (11) is essential for others, as discussed in Sec. VI.

III. SINGLE ELECTRON SPECTRUM

We consider the electron kinetic energy to arise both from nearest neighbor (NNH) and second neighbor (SNH) hopping between carbon atoms as depicted in Fig. 2. The hopping integrals are modulated by the lattice distortions providing thus the electron-lattice interaction. (An additional effect would, e.g., follow from the modulation of Coulomb repulsion between extra charges.) As is customary, a linear modulation with distances is assumed. So NNH integrals are modulated as

$$t_a = t_0 - \alpha\delta_a, \quad t_b = t_0 - \alpha\delta_b, \quad t_c = t_0 - \alpha\delta_c, \quad (12)$$

where t_0 is the NNH integral on the undistorted lattice and α the NNH coupling constant. Similarly, SNH integrals t_1, t_2, and t_3 are modulated with the SNH distances, the modulation strength given by the SNH coupling constant β. We expect $\beta/\alpha \sim 0.1$. Expressing changes of distances in terms of introduced distortion modes (4) will yield the corresponding coupling constants for each of the modes, as done below. With SNH included, the charge conjugation symmetry of the half-filled system is broken and the band energies have the form

$$\epsilon_\pm(\vec{k}) = \tau(\vec{k}) \pm \xi(\vec{k}) \quad (13)$$

for the conduction and valence bands, respectively, where $\xi(\vec{k})$ originates from the NNH and $\tau(\vec{k})$ from the SNH, and $\vec{k} = (k_x, k_y)$ is the 2-d dimensional wave vector. With the definitions of Fig. 2,

$$\tau(\vec{k}) = -2t_1 \cos k_x a - 2t_2 \cos k_- a - 2t_3 \cos k_+ a, \quad (14)$$

$$\xi^2(\vec{k}) = t_a^2 + t_b^2 + t_c^2 + 2t_a t_c \cos k_x a + 2t_a t_b \cos k_- a + 2t_b t_c \cos k_+ a, \quad (15)$$

where $k_\pm = (k_x \pm \sqrt{3}k_y)/2$. For not too small diameter nanotubes the low excitation energy region is always close to the special, ''Dirac,'' points in the momentum space, where the gap between the valence and conduction states of the (isotropic) graphene spectrum [as determined by Eq. (15)] vanishes. Then one can use expansions of the exact band energies (14) and (15) in momenta around the special points and in (small) deviations of hopping integrals around their bare values. For certainty, we choose the special point $\vec{K} = (4\pi/3a, 0)$ and, from now on, all momenta $\vec{k} = (k_x, k_y)$ will be measured with respect to that special point ($k_x \to 4\pi/3a + k_x$). [It should be clear that the other inequivalent special point could be $\vec{K}' = (-4\pi/3a, 0)$, which, in view of the even dependence of spectrum (13) on electron quasimomenta, results just in a factor of 2 taken into account below in the summation over the relevant electron states.] After some exercise, one reduces Eqs. (14) and (15) to

$$\tau(\vec{k})/t_0 = \tau_0(\vec{k})/t_0 + \sqrt{3}(\beta/\alpha)\{\hat{S} + 3[k_x(\hat{A}_1 + \hat{B}_2) + k_y(\hat{A}_2 - \hat{B}_1)]a/4\}, \quad (16)$$

$$\xi^2(\vec{k})/t_0^2 = (3 + 2\hat{S} - 2\sqrt{3}\hat{A}_1)(k_x a - \hat{A}_1)^2/4 + (3 + 2\hat{S} + 2\sqrt{3}\hat{A}_1)(k_y a - \hat{A}_2)^2/4 + \sqrt{3}\hat{A}_2(k_x a - \hat{A}_1)(k_y a - \hat{A}_2). \quad (17)$$

Here τ_0 is the equilibrium value of τ and we introduced dimensionless variables $\hat{S} = -\alpha S/t_0$, $\hat{A}_1 = -\alpha A_1/t_0$, $\hat{A}_2 = -\alpha A_2/t_0$, $\hat{B}_1 = -\alpha B_1/t_0$ $\hat{B}_2 = -\alpha B_2/t_0$ to save space in formulas (the same would be used for rotated modes $A_\parallel$ and $A_\perp$. Applicability of expansions (16) and (17) requires $k_x a \ll 1$ and $k_y a \ll 1$ as well as relatively small distortion amplitudes. In view of this and the smallness of β/α, one can safely neglect the terms in Eq. (16) that are proportional to $ka \ll 1$.

For the (N,M) tube, the chiral angle ϕ (Figs. 1 and 2) is defined through $\sin\phi = (N-M)/2C_h$, where the dimensionless tube circumference $C_h = (N^2 + M^2 + NM)^{1/2}$ (it is related to the tube radius as $2\pi R = aC_h$). We consider ϕ belonging to the interval between 0 (armchair tubes) and $\pi/6$ (zigzag tubes). The angle ϕ is complementary to the chiral angle θ as defined in Ref. 1: $\phi = \pi/6 - \theta$. Of extreme importance is the divisibility of $N-M$ by 3, the ''remainder'' $q = 0, \pm 1$ is introduced by

$$N - M = 3m + q, \quad (18)$$

where m is the appropriate integer. The electron momenta can lie only on a set of quantization lines, the one most closely approaching the special point is described by

$$k_x \sin\phi + k_y \cos\phi = -2\pi q/3C_h a = K_0/a. \quad (19)$$

According to Eq. (17), the lowest ξ-energy in the equilibrium system is $\xi_0 = t_0(3K_0^2/4)^{1/2} = |q| t_0 d/2R$, finite for semiconducting nanotubes ($|q|=1$), and zero for metallic ones ($q=0$).

One-dimensional (momentum k) "ξ bands" along the quantization lines are obtained from Eq. (17) and have the familiar Dirac form

$$\xi^2(k) = \Delta^2 + v_\parallel^2 k^2, \tag{20}$$

where the gap parameter

$$\Delta = v_\perp |K_0 - \hat{A}_\perp|/a \tag{21}$$

and the effective Fermi velocities

$$v_\parallel = v_F - a t_0 \hat{A}/2, \quad v_\perp = v_F + a t_0 \hat{A}/2. \tag{22}$$

Here $v_F/at_0 = \sqrt{3}/2 + \hat{S}/2\sqrt{3}$, and the dimensionless $\hat{A}$ is defined through dimensionless $\hat{A}_\parallel$ and $\hat{A}_\perp$ as in Eq. (6). Higher lying energy bands are evidently also described by Eq. (21), where the q used in the definition of K_0 would be "displaced" by $3m$, where m is an integer. If, e.g., the lowest energy band corresponds to $q=-1$, the first higher lying band would be with $q=2$, still the next with $q=-4$, and so on.

The curvature affects the effective 2-d description of the electron spectrum of nanotubes. As we discussed in Sec. II, even in the ground states, nanotubes are deformed with respect to graphene. In our applications, it means that all distortion modes in Eqs. (16) and (17) and further on would have to be displaced like $S \to S_R + S$, $A_\parallel \to A_R \cos 3\phi + A_\parallel$, etc. In addition, the curvature changes the overlap of π-orbitals which can be represented as another source of the effective external distortion $A_R \to A_R + A_e$, $S_R \to S_R + S_e$, $S_e = \sqrt{3} A_e$, so that bonds along the tube axis do not change while the other bonds change their length appropriately. An elegant analysis of the modulation of the NNH by curvature was, e.g., given by Kane and Mele,[16] from their work we deduce the value $A_e = t_0 \pi^2/4\sqrt{3}\alpha C_h^2$. In our calculations below, we will be taking into account only the anisotropy term A_e as responsible for curvature-derived gaps in quasimetallic tubes.

IV. MODULATION OF THE GAP BY DEFORMATIONS

The modulation of the gap energy $E_g = 2\Delta$ by the longitudinal $\gamma_\parallel$ and torsional η strain is the effect whose extensive analysis was given in Ref. 10, where references to earlier work can also be found. Here we discuss it within our framework, indicating differences with the treatment of Ref. 10 and giving a simple physical picture for the peculiar features of the effect.

Equation (21) shows how the gap parameter Δ is modulated by the bond-stretching modes $S, A_\parallel$, and $A_\perp$. When strains $\gamma_\parallel$ and/or η are applied, they cause lattice distortions so as to minimize the elastic energy (7): in general both bond-stretching and bond-bending modes are excited but the latter do not affect the gap. The isotropic displacements are simply determined by $S = 3\gamma_0 d$, while the anisotropic displacements are related to the shear strain components

$$\begin{aligned} A_\parallel &= -\sqrt{3} z_a (\gamma \cos 3\phi + \eta \sin 3\phi) d, \\ A_\perp &= -\sqrt{3} z_a (\gamma \sin 3\phi - \eta \cos 3\phi) d. \end{aligned} \tag{23}$$

Using equilibrium $\gamma_0 = (1-\nu)\gamma_\parallel/2$ and $\gamma = (1+\nu)\gamma_\parallel/2$, it is now straightforward to find the gap modulation δE_g of semiconducting tubes ($q = \pm 1$) at small strains:

$$\frac{\delta E_g}{\alpha d} = \frac{\pi(\nu - 1 + (1+\nu) z_a)}{\sqrt{3} C_h} \gamma_\parallel \tag{24a}$$

$$+ 3 q z_a [(1+\nu)\gamma_\parallel \sin 3\phi - 2\eta \cos 3\phi]/2. \tag{24b}$$

Apart from the difference in notation, Eq. (24b) agrees with the result of Ref. 10 on the chiral dependence of the major modulation effect. Noteworthy is the appearance of the factor z_a in Eqs. (23) and (24), which would be 1.28 with numbers (8). Analytical calculations of Ref. 10 assume that the lattice deforms under strain as if it was a 2-d elastic continuum. The factor z_a accounts for the difference caused by the actual elastic properties of the lattice, this factor becomes unity[11] when the difference effectively disappears. In the extreme case of $K_B = K_{AB} = 0$, the factor z_a becomes 0, and the largest part of the gap modulation (24b) disappears because the shear deformation would be realized only through the bond-bending modes. In the opposite extreme case of $K_B = \infty$, all the shear occurs through bond-stretching modes and the factor $z_a = 2$. Reference 10 provides numerical results on modulation for a specific choice of the coupling constant α. Equation (24a) reflects a correction $\propto 1/R$ coming from the modulation of the Fermi velocity in Eq. (21).

The notable feature of Eq. (24b) is the factor q which leads to oscillations of the responses of the semiconducting tubes as a function of $N-M$. Consider, e.g., zigzag tubes that have the strongest response to the longitudinal strain. The longitudinal extension of the (10, 0) tube with $q=1$ results in a gap increase, while the extension of the (11, 0) tube with $q=-1$ results in a gap decrease. We find that a very transparent physical picture can be offered to understand this fascinating behavior. Let us calculate the contributions to the gap energy of the semiconducting tubes coming from different types of nearest neighbor carbon-carbon bonds, i.e., the matrix elements of the corresponding parts of the Hamiltonian at the conduction band minimum wave vectors [$k_x a = K_0 \sin\phi$, $k_y a = K_0 \cos\phi$; see Eq. (19)]. The problem is equivalent to finding the phase factors for three vectors representing the three types of bonds that maximize the conduction-valence band splitting. One readily derives that the bonds d_i contribute $-\cos(\varphi + \phi_i)$ to Δ/t_0, where $\varphi = -q\pi/2 - \phi$, $\phi_a = 2\pi/3 + K_0 \sin(\phi - \pi/6)/\sqrt{3}$, $\phi_b = K_0 \cos\phi/\sqrt{3}$, and $\phi_c = -2\pi/3 - K_0 \sin(\phi + \pi/6)/\sqrt{3}$. Table I gives numerical examples of the bond contributions for four tubes. We will call "bonding" those bonds whose contribution is negative and "antibonding" those whose contribution is positive. By definition, an expansion of the bonding bonds increases the gap, and their contraction decreases the gap; effects for the antibonding bonds are the opposite. Table

TABLE I. The bonding patterns for four tubes. The contributions from bonds d_a, d_b, and d_c are normalized so that their sum gives the gap parameter in units of t_0.

Tube	d_a	d_b	d_c	Δ/t_0
(10,0)	−1.0	0.588	0.588	0.176
(11,0)	1.0	−0.415	−0.415	0.169
(10,5)	0.954	−0.1	−0.715	0.139
(10,6)	−0.916	0.227	0.818	0.128

I illustrates a dramatic difference of the bonding patterns of tubes with $q=1$ and -1. Indeed, the bond d_a along the tube axis of the zigzag tubes turns out to be bonding for the (10, 0) tube and antibonding for the (11, 0) tube, leading to effects in agreement with Eq. (24b). By the same token, it is clear that a twist of a certain direction would result in opposite effects on the gap for tubes (10, 5) and (10, 6).

For quasimetallic tubes ($q=0$), the gap modulation is given by $\delta E_g=\sqrt{3}\alpha s_0 A_\perp$, where $s_0=\sin(A_e\sin 3\phi+A_\perp)$ with $A_\perp$ from Eq. (23) and $\gamma=(1+\nu)\gamma_\parallel/2$. In the absence of the curvature-induced gap ($A_e\sin 3\phi=0$), of course, strains could only produce a finite gap. With the curvature-derived gap in place, there would be a range of relatively small strains where the gap can be decreased. We note that a small longitudinal extension $\gamma_\parallel>0$ particularly leads to such an effect. It is intuitively clear that the curvature makes hopping integrals ''perpendicular'' to the tube axis smaller than those ''parallel'' to the axis. The curvature-derived gap would be decreased if all the hopping integrals become more equilibrated, and for this one needs a longitudinal extension and/or transverse contraction.

V. CHARGE-INDUCED DISTORTIONS

Suppose one adds δn extra electrons ($\delta n<0$ for holes) per carbon atom to a SWNT. How would interatomic distances be affected? Here we study the contribution to bond length changes arising from the modulation of electron hopping integrals t by lattice distortions. The basic illustration is very simple: if an extra electron or hole is added to a half-filled two-site system, this would cause an expansion of the intersite bond by $\delta d=\alpha/K$, where K is the elastic constant and the hopping integral is modulated as $\delta t=-\alpha\delta d$. We will show that this relaxation mechanism can produce surprisingly different results for carbon nanotubes having different values of N and M.

To evaluate the lattice deformation to accommodate additional charges on the nanotube, we need to know the energy $E_{\rm el}$ of extra charges as a function of the distortion coordinates. It is well known that one-dimensional electron-phonon systems can be unstable with respect to the Peierls distortion, and exhibit the formation of nonuniform polaronic distortions. For *not very small* carbon nanotubes, however, these effects seem practically irrelevant. The estimated transition temperatures (e.g., Ref. 17) and polaron binding energies[17,18] are on the order of 1 K or smaller. So even quite low temperatures in excess of those estimates are sufficient to prevent nonuniform charge distributions. Of course, quantum fluctuations also act to render polaronic states unstable. With a uniform distribution of excess charges over the lattice sites and relatively low temperatures, it will be safe to assume that electrons or holes added to the system are accommodated in the band states of the lowest available excitation energies. (In fact, the authors of Ref. 18 in a recent publication[19] also used the band states to be filled by extra charges.) The lattice displacements affect $E_{\rm el}$ through the variation of the band parameters, as discussed in Sec. III.

With only one (with account of degeneracy) electronic band being filled, the variable part of the electronic energy per carbon takes the form

$$E_{\rm el}=\sqrt{3}(\beta/\alpha)S\delta n+(1/f)\int_0^{\delta k}\xi(k)\mathrm{d}k, \tag{25}$$

where only one practically non-negligible term from Eq. (16) is left. The coefficient f relates the boundary δk of the occupied states in the momentum space to the charge injection level: $\delta k=f|\delta n|$, $f=\pi C_h/a\sqrt{3}$.

The lattice energy is given by Eq. (7), and the resulting distortion pattern is obtained by minimization of the total energy (1). Equation (25) is independent of B_i distortion modes which then acquire a finite value only through the elastic coupling to A_i modes in Eq. (7). Substituting those derived values in Eq. (7) then leads to the effective lattice potential energy in terms of S and A_i modes only:

$$U=K_S S^2/2+K'_A(A_\parallel^2+A_\perp^2)/2, \tag{26}$$

where $K'_A=K_A-K_{AB}^2/K_B$. With parameters (8), $K'_A=4.35$ eV/Å^2. The dimensional changes (5) then would be

$$d\cdot\gamma=-uA/2\sqrt{3},\quad d\cdot\eta=uC/2\sqrt{3} \tag{27}$$

where the correction factor $u=1-K_{AB}/K_B=0.83$ if (8) is used.

As an instructive example, we first analyze the effects linear in δn. Then the second term in Eq. (25) reduces to $\Delta|\delta n|$. Let us neglect all the curvature effects for this illustration. The minimization of the total energy is trivial, and yields the optimal distortion patterns

$$\frac{K_S S}{|\delta n|}=\pm\sqrt{3}\beta+\frac{\pi\alpha|q|}{3\sqrt{3}C_h}, \tag{28a}$$

$$\frac{K'_A A_\parallel}{|\delta n|}=\frac{\pi\alpha|q|}{3C_h}\cos 3\phi, \tag{28b}$$

$$\frac{K'_A A_\perp}{|\delta n|}=\frac{\pi\alpha|q|}{3C_h}\sin 3\phi+\sqrt{3}\alpha q/2. \tag{28c}$$

This corresponds to the following macroscopic distortions:

$$\gamma_0=\frac{1}{\sqrt{3}K_S d}\left(\pm\beta+\frac{\pi\alpha|q|}{9C_h}\right)|\delta n|, \tag{29a}$$

$$\gamma = -\frac{u\alpha}{4K_A' d}\left(\frac{\pi|q|}{6\sqrt{3}C_h} + q\sin 3\phi\right)|\delta n|, \qquad (29b)$$

$$\eta = \frac{u\alpha}{4K_A' d} q\cos 3\phi\,|\delta n|, \qquad (29c)$$

upper and lower signs in Eqs. (28) and (29) stand for electron and hole doping.

Of course, the most interesting are the proportional to q terms in Eqs. (29b) and (29c) that lead to responses oscillating as a function of $N-M$. For semiconducting tubes, these terms are dominating, and they establish a large scale anisotropy of the axial ($\gamma_\parallel = \gamma_0 + \gamma$) and radial ($\gamma_\perp = \gamma_0 - \gamma$) responses. The electron-hole symmetric effect here is inverse to the gap modulation effect discussed in the previous section: extra charges at the band extremum want to decrease their energy by decreasing the gap. The bonding picture illustrated in Table I helps to understand the peculiar oscillations and anisotropy. So for the (10, 0) tube ($q=1$, $3\phi = \pi/2$) the bonds along the tube axis are bonding; they therefore shrink upon charge injection. The bonds ''perpendicular'' to the tube axis are antibonding and they would expand. This picture reverses for the tube (11, 0) with $q=-1$, in full agreement with Eq. (29b). We note that these peculiar effects in Eqs. (29b) and (29c) result exclusively from the excitation of the $A_\perp$ mode (28c) that directly modulates the gap (21).

Figure 3 displays equilibrium deformations of a series of nanotubes for the electron doping level $\delta n = 0.5\%$ calculated through a numerical optimization of the total energy. The figure shows not only the linear effects [Eqs. (29)] but also the interplay of effects coming from the curvature and the filling of the electron states above the band edge. The appearance of a small gap $\propto A_e$ drastically changes the responses of quasimetallic nanotubes for very low doping levels. However, the role of a small gap quickly diminishes upon increase of the doping level. For calculations, in addition to the elastic constants (8), we used electronic parameters: $\alpha = 5$ eV/Å and $\beta/\alpha = 0.2$. The results are practically independent of the value of t_0. The salient qualitative features—an oscillating character of the responses as a function of the nanotube geometry and a large scale anisotropy of the dimensional changes—are clearly seen.

A further increase of the injection level leads to charges starting to fill in the higher lying energy bands. The lowest critical densities are found as $\delta n_{\rm met} = 2\sqrt{3}/C_h^2$, $\delta n_{\rm sem} = 2/C_h^2$. This yields, e.g., $\delta n_{\rm met} \simeq 1.2\%$ for the (10, 10) nanotube, and $\delta n_{\rm sem} \simeq 1.7\%$ for the (11, 0) nanotube. The onset of the filling in the next higher lying bands leads to sudden changes (they would be smoothed by finite temperatures) in the responses—obviously, a distortion $A_\perp$ that decreases gap (21) for the first band (say, with $q=1$) would increase the gap for the second band (with $q=-2$). ''Conflict of interests'' of different bands are studied with the single band integral in Eq. (25) replaced with $\Sigma_i \int_0^{\delta k_i} \xi_i(k)\mathrm{d}k$ over multiple bands i with appropriate boundaries δk_i. In Fig. 4 we show calculated $\gamma_\parallel$ for a series of carbon nanotubes as a function of the injection level. Sharp changes in the responses are clearly seen for the tubes (16, 0) and (17, 0), whose critical densities are within the displayed injection range. In these simplified calculations, we neglected possible changes of critical densities and δk_i caused by the lattice deformations.

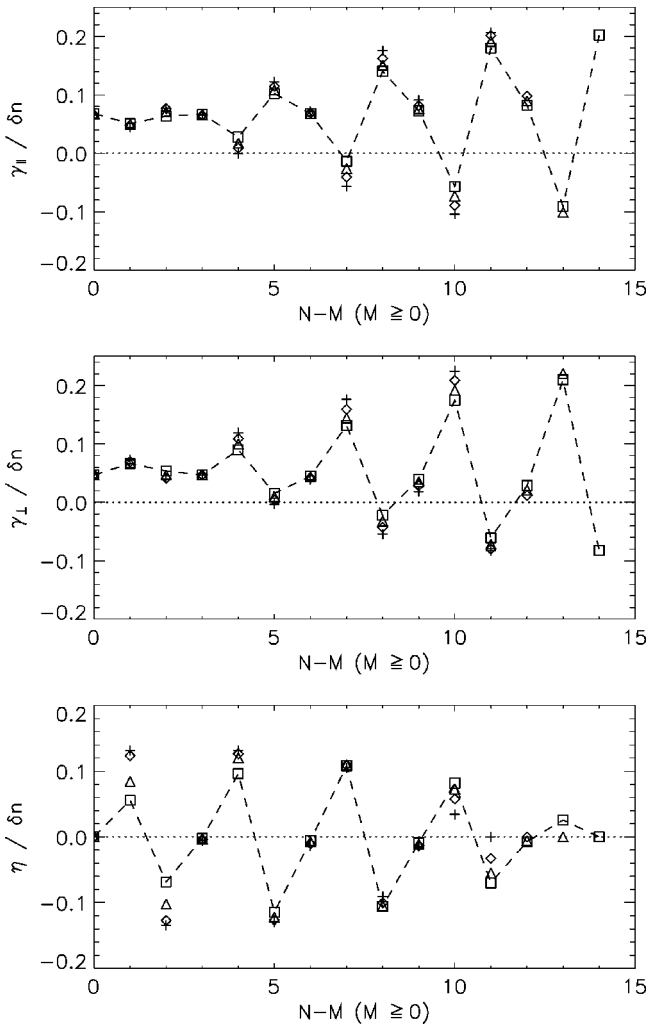

FIG. 3. Deformations of nanotubes for the electron doping level $\delta n = 0.5\%$. Shown are results for four ''families'' of carbon nanotubes: with $N=11$ (crosses), 12 (diamonds), 13 (triangles), and 14 (squares). The square data points are connected with broken lines. The upper panel shows changes in the nanotube length, the middle panel shows changes in the nanotube radius, and the lower panel shows torsional shear.

Within the same model, the dimensional response of graphite would be a smooth curve[20]

$$\gamma_0 = \frac{1}{\sqrt{3}K_S d}\left[\beta\delta n + \alpha\frac{2}{\pi}\left(\frac{\pi|\delta n|}{3\sqrt{3}}\right)^{3/2}\right], \qquad (30)$$

while $\gamma = \eta = 0$. In graphite, it is only the isotropic mode that gets excited upon charge injection leading to the isotropic expansion/contraction of the lattice. The second neighbor effect $\propto\beta$ in Eq. (30) provides for charge conjugation symmetry breaking between electron and hole doping, and is the same as in the nanotubes independently of their geometry [Eq. (29a)]. This term is important to account for the

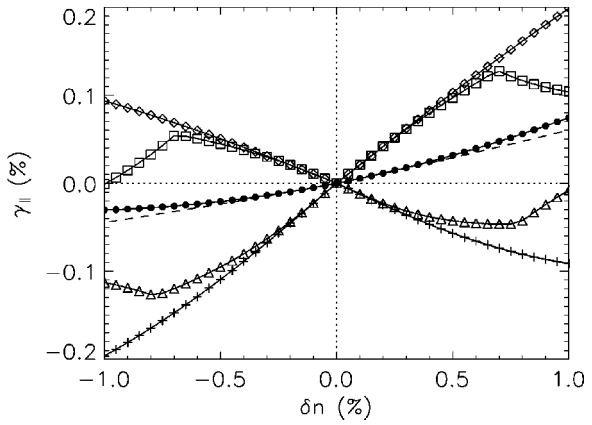

FIG. 4. Longitudinal dimensional changes for a series of doped nanotubes as a function of the injection level. Note that in this figure as well as in Figs. 5 and 6, the injection level is shown in percent ($\delta n = 0.01$ is equivalent to $\delta n = 1\%$). A positive δn corresponds to electron doping and a negative δn to hole doping. Crosses are for the (10, 0) zigzag tube, diamonds for the (11, 0) tube, triangles for the (16, 0) tube, squares for the (17, 0) tube, and filled circles for the (10, 10) armchair tube. Lines just connect the calculated data points. The dashed line shows result (30) for graphite.

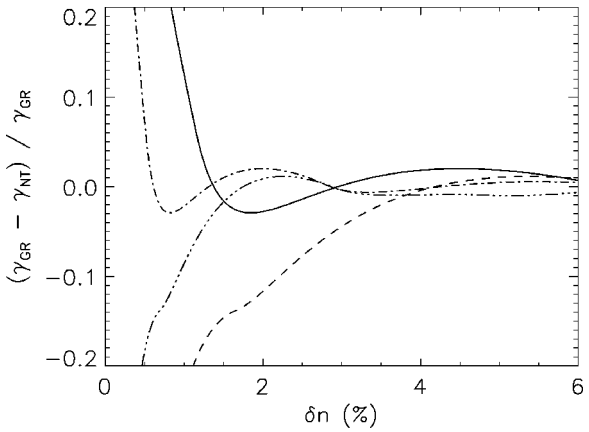

FIG. 5. Relative deviations of the isotropic NNH part of nanotube responses (γ_{NT}) from that of graphite (γ_{GR}) as a function of the charge injection level. Results are shown as follows: with the solid line for the (10, 10) tube, with the dashed line for the (11, 0) tube, with the dash-dotted line for the (15, 15) tube, and with the dash-dot-dotted line for the (17, 0) tube.

electron-hole doping asymmetry of graphite intercalation compounds, as suggested in earlier work.[14,21,22] Experiments on electrochemical actuators with carbon nanotubes[6] also indicated an asymmetric response. Being linear in the doping concentration δn, this term can be dominating for graphite and quasimetallic tubes with $q = 0$ (at least for the armchair tubes). The strong electron-hole asymmetry of the graphite and armchair nanotube responses caused by the modulation of SNH is clearly seen in Fig. 4.

On the other hand, the electron-hole symmetric NNH modulation (modulation of the Fermi velocity) in graphite results in the second term in Eq. (30) $\propto \alpha$. Similar isotropic parts are also present in the nanotube responses [see, e.g., the second term in Eq. (29a)]. They, however, have a different functional dependence on δn. It is interesting to see how those parts converge to the $\propto |\delta n|^{3/2}$ behavior of the graphite with increasing doping and/or with increasing nanotube size. Figure 5 illustrates this convergence as relative deviations of the corresponding parts of the responses. In fact, there are two universal behaviors there: one for metallic tubes and one for semiconducting tubes; the curves within each class transform into each other with δn scaling as C_h^{-2}, where C_h is the tube circumference.

Of course, much larger deviations from the graphite behavior can occur due to anisotropic modes. These take place even for metallic tubes, but, for semiconducting tubes at low doping levels, the electron-hole symmetric NNH gap modulation is especially significant leading to dimensional responses that can be substantially larger than graphite's. The nanotube strains caused by charge injection may generally be thought of as ''fluctuating around'' the graphite response, exhibiting the sharp transitions described above. The amplitude of the fluctuations and the spacing between them decrease with the size of the nanotubes, gradually approaching the graphite response as $N, M \to \infty$. With the increasing injection level, relative deviations from the graphite curve also become smaller.

It is the quantization of electronic states in nanotubes that makes anisotropic distortion modes a prominent feature of the accommodating lattice relaxation. An excitation of the anisotropic distortion modes causes the macroscopic shear deformations. The anisotropy of the longitudinal and transversal responses of nanotubes is one consequence; the other is the torsional deformations. At very low injection levels, the behavior of the latter is shown in Eq. (29c), numerical results for higher doping levels are shown in Figs. 3 and 6. As we discussed, the onset of filling in higher energy bands causes sudden changes in responses, clearly seen in Fig. 6 for twisting deformations.

For numerical calculations in this paper, we chose to increase the parameter β/α because of the increased stiffness

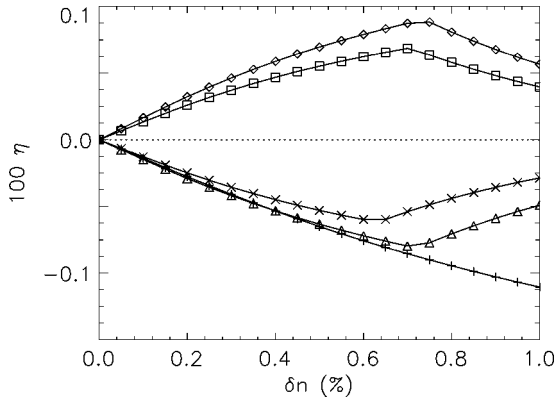

FIG. 6. Torsional shear deformations for a series of electron doped chiral semiconducting nanotubes as a function of the injection level. Crosses are for the (10, 5) tube, diamonds for the (10, 9) tube, triangles for the (12, 7) tube, squares for the (13, 6) tube, and x's for the (14, 6) tube. Lines here just connect the calculated data points.

K_S, as compared to parameters used in Ref. 7, and in order to keep the results for graphite closer to experimental data (see, e.g., a compilation in Ref. 14). Of course, numerically results are affected by the choice of parameters; however, the salient qualitative features distinguishing the behavior of nanotubes from graphite are quite robust. We hope that a more accurate parametrization of the model can be achieved by fitting to results of *ab initio* calculations, such as in Ref. 14, and to experimental data, which is not attempted here.

The behavior discussed above arises at low temperatures in the single-electron picture. Thermal excitation of charges into higher lying energy bands will likely be bringing nanotube responses closer to that of the graphite's, as well as decreasing the sharpness of transitions. However, since the separation between energy bands is large compared with the room temperature thermal energies for not-too-large tubes, we expect the thermal corrections to be relatively small. Also, superimposed on the discussed effects can be a uniform expansion $\propto \delta n^2$ coming from the Coulomb repulsion of extra charges, whose magnitude depends on the positioning of counterions and dielectric properties of the medium. Coulombic intratube repulsion may dominate actuation when charge injected is large. This repulsion will, however, be absent in the system where extra electrons and holes are introduced as a result of photoexcitation and then quickly relax to the band edges and spend some time there. Evaluation of the *e-e* correlation effects would require further studies.

VI. STRETCH-INDUCED TORSION

In this section we deal with purely mechanical coupling: conversion of the tensile strain into torsion,[8] the effect very familiar for ordinary helical springs. In our effective 2-*d* treatment, the tensile longitudinal deformation is described by the strain $\gamma_\parallel$ and the torsion $\delta\phi_l = \eta/\pi R$ by the η component of the shear tensor. The problem of the stretch-induced torsion can then be posed as finding the equilibrium η for a given $\gamma_\parallel$. It is quite clear that in an isotropic system with rotationally invariant elastic energy [Eq. (9)], the resulting optimal deformation for a given $\gamma_\parallel$ would have $\eta = 0$ and the stretch-induced torsion would not occur in the corresponding tube. The effective 2-*d* system has to be *anisotropic* for the optimal η not to vanish. Also, the system has to have lifted the reflection symmetry around the nanotube axis: $U_{\rm m}(\gamma_0, \gamma, \eta) \neq U_{\rm m}(\gamma_0, \gamma, -\eta)$, we can relate this to *chirality* of the system. Nanotubes readily give examples of such systems.

Two main questions are to be clarified. (1) How does η depend on the tube radius R? General scaling arguments for not-too-small tubes with short-range elastic interactions require η to be an even function of $1/R$: $\eta = \eta_0 + \eta_2/R^2 + \eta_4/R^4 + \cdots$; η_0 here reflects the magnitude of the bare elastic anisotropy of the unwrapped sheet and equals to zero when the latter is elastically isotropic, while $\eta_2, \eta_4, \ldots$ are curvature derived effects.[23] Correspondingly, the large $-R$ scaling for the systems with bare anisotropy (like type-II BC_2N tubes[9]) is $\delta\phi_l \propto 1/R$ and for the systems with curvature-derived anisotropy (like carbon nanotubes) is $\delta\phi_l \propto 1/R^3$.[24] (2) How does η depend on the relative orientation of the tube axis, or on the chiral angle ϕ? This dependence relates to the symmetry properties of the unwrapped sheet and/or to the symmetry breaking introduced by the wrapping.

Let us study the latter for carbon nanotubes. One can use the optimized microscopic distortions for a given macroscopic deformation (γ_0, γ, η) to derive the following macroscopic elastic anisotropy per carbon from Eq. (11):

$$\delta U_{\rm m} = C_0^a \gamma_0 \gamma + \frac{C_{\rm sh}^a}{2}[(\gamma^2 - \eta^2)\cos 6\phi + 2\gamma\eta \sin 6\phi]. \tag{31}$$

The functional form [Eq. (31)] is required by the symmetry of the axial anisotropy on a hexagonal background and can be also obtained directly using the same symmetry considerations.[15] Note that five anisotropy parameters of Eq. (11) have been reduced to only two. For small anisotropy, the effective anisotropy energies are found as $C_0^a = 3d^2(z_b K_{SB}^a - z_a K_{SA}^a)$ and $C_{\rm sh}^a = 3d^2(z_a^2 K_A^a - z_b^2 K_B^a + 2 z_a z_b K_{AB}^a)$. Both energies are curvature derived and scale as $1/R^2 + \cdots$.

Optimizing $U_{\rm m} = U_{\rm m}^0 + \delta U_{\rm m}$ for a given $\gamma_\parallel$ and small anisotropy, we find the equilibrium η shear as

$$\eta/\gamma_\parallel = -(1+\nu) C_{\rm sh}^a \sin 6\phi / 2 C_{\rm sh}. \tag{32}$$

Equation (32) indicates that maximum torsion for tubes of the same radius occurs at the chiral angle $\phi = \pi/12$, in the middle between armchair and zigzag tubes, and vanishes for achiral tubes, in agreement with results of molecular dynamics simulations.[8]

We now want to relate the curvature-derived stretch-induced torsion in Eq. (32) to another effect, the chirality dependence of the stiffness of nanotubes that was discussed in Refs. 25 and 13. With the same $U_{\rm m}$ we calculate anisotropy corrections to the longitudinal stiffness as

$$\frac{\partial^2 U_{\rm m}}{\partial \gamma_\parallel^2} = C + \frac{(1-\nu^2)}{2} C_0^a + \frac{(1+\nu)^2}{4} C_{\rm sh}^a \cos 6\phi, \tag{33}$$

where C is the contribution coming from $U_{\rm m}^0$ and discussed in Sec. II. All C energies in Eq. (33) are R dependent. The coefficient $C_{\rm sh}^a$ in (33) that provides for a chirality dependence is the same that determines the torsional shear in (32). Eq. (33) predicts a monotonic dependence of the stiffness on the chiral angle between 0 and $\pi/6$, which was indeed found in empirical calculations.[25] Comparing Eq. (33) to results of Ref. 25, we conclude that $C_{\rm sh}^a > 0$ and is substantial in the sense that its magnitude is comparable to the overall R dependence of the longitudinal stiffness. The absolute magnitude of these effects, however, may strongly depend on the details of the empirical model used for calculations. Reference 25 found very significant variations of the stiffness with the radius of nanotubes when using the Tersoff interatomic potential and much smaller with the Brenner potential; *ab initio* calculations[13] also indicate a weak R dependence of the stiffness. Molecular dynamics simulations of Ref. 8 yield

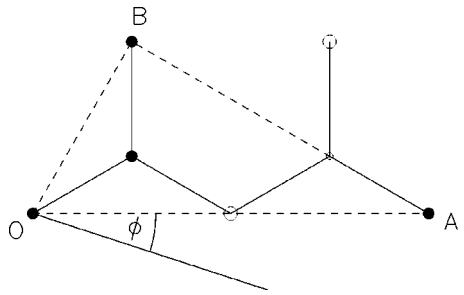

FIG. 7. Element of the type-II BC_2N tube structure with four atoms in the unit cell. Solid circles denote C atoms while large and small open circles denote respectively N and B atoms. See Ref. 9 for details of the full structure.

~ 0.01 for the ratio (32) for the (10, 5) tube. The direction of the twist found[8] agrees with the sign of $C^a_{\rm sh}$ deduced from the stiffness calculations.[25]

One could expect a much larger stretch-induced torsion effect in the tubes which are elastically anisotropic already in the unwrapped sheet state. An example of such may be type-II BC_2N tubes (see Fig. 7), where an anisotropy is expected by virtue of the different interatomic interactions between different types of atoms. We therefore restrict our attention to the η_0 term. As is clear from Fig. 7, the symmetry element left on the parent sheet is the reflection around the *AB* axis. Using this as a general symmetry constraint, one derives the anisotropic part of the elastic energy as

$$\delta U_{\rm m} = C^a_0 \gamma_0 (\gamma \cos 2\phi_1 + \eta \sin 2\phi_1) + \frac{C^a_{\rm sh}}{2}[(\gamma^2 - \eta^2)\cos 4\phi_1 + 2\gamma\eta \sin 4\phi_1], \quad (34)$$

where $\phi_1 = \phi - \pi/6$ and C^a_0 and $C^a_{\rm sh}$ are some anisotropy energies. Optimizing $U_{\rm m}$ now for a given $\gamma_\parallel$ and small anisotropy leads to the following chiral dependence of the effect:

$$\eta/\gamma_\parallel = -[(1-\nu)C^a_0 \sin 2\phi_1 + (1+\nu)C^a_{\rm sh}\sin 4\phi_1]/2C_{\rm sh}. \quad (35)$$

It follows from Eq. (35) that the torsional shear vanishes for $\phi = \pi/6$ and $\phi = 2\pi/3$, that is, along respectively *AB* and *OB* vectors in Fig. 7, as one should expect. In addition, the system may have another couple of such directions depending on the anisotropy parameters. The latter determine the sign and magnitude of the torsion. Some information on elastic properties of BC_2N tubes is available from *ab initio* calculations[26] but not sufficient for us to make estimates.

Torsion of nanotubes can also be caused by hydrostatic-like forces that would result in the isotropic lattice expansion/contraction in the absence of the anisotropy. One can find equilibrium η for a given γ_0 describing the isotropic effect. With the curvature-derived anisotropy energy [Eq. (31)] of carbon nanotubes, a finite η appears only in the second order of the anisotropy parameter,

$$\eta/\gamma_0 = (C^a_0 C^a_{\rm sh}/C^2_{\rm sh})\sin 6\phi,$$

and, therefore, is expected to be minuscule. In contrast, the inherent anisotropy energy [Eq. (34)] of BC_2N tubes leads to a finite effect already in the first order,

$$\eta/\gamma_0 = -(C^a_0/C_{\rm sh})\sin 2\phi_1,$$

and could be observable.

VII. SUMMARY

We have developed a simple framework for an effective description of the static lattice deformations for the hexagonal atomic structure of carbon nanotubes, as well as of the actuation responses related to those deformations. For single walled nanotubes of arbitrary geometry, we analyzed dimensional and torsional deformations caused by charge injection and the torsional rotations induced by stretching. The dimensional changes induced by charge injection are the basis for carbon nanotube electromechanical actuators (artificial muscles). Since the predicted actuation is a sensitive function of structure when the amount of charge injection is small, these actuation results may be important for optimization of nanotube actuators for targeted applications. However, present assemblies of many nanotubes, such as long fibers and sheets, are polydispersed in nanotube type—so an average response is likely to be obtained which is more graphite-like.

Shear (anisotropic) deformations play an important role for individual nanotubes leading to large and fascinating deviations from the behavior of graphite. It has been recognized that anisotropic deformations can introduce symmetry breaking[16] and modulate the gap energy[10] in nanotubes. We have shown that charge injection can conversely result in shear deformations that would significantly effect the produced dimensional changes. Charge-induced strains exhibit a strong ''oscillatory'' dependence on the nanotube geometry (N,M). Deviations from the charge induced strain of graphite are predicted to be particularly large for semiconducting tubes at low injection levels. A large anisotropy of dimensional changes is expected, which may lead, e.g., to a decreasing diameter and increasing length upon charge injection. For the same sign of carrier injection, some tubes may experience a longitudinal expansion and others a contraction. A similar oscillatory dependence is also predicted for the charge-induced torsional twists. Even the electronic band structure of the nanotubes can reveal itself through (sharp) changes of the actuation responses as a function of the charge injection level. We found that the peculiar oscillatory behavior of the semiconducting tubes' responses can be easily understood in terms of the bonding pattern, near the band minima, which changes with $N-M$. Dimensional changes in the fiber direction during charge injection can be most enhanced for semiconducting zigzag tubes. On the other hand, charge-induced torsional rotations have the largest magnitude for chiral semiconducting nanotubes.

The curvature-induced isotropy breaking of elastic interactions in carbon nanotubes also gives rise to the stretch-induced torsional rotations about the nanotube axial direction. We showed that this stretch-torsional coupling may be

enhanced using chiral nanotubes in which the anisotropy of elastic interactions is increased through substitution of carbon atoms.

Quantitative predictions of our model depend on the values of several parameters, such as effective elastic constants and electron-lattice interaction constants, for which we used reasonable estimates. While the magnitude of predicted effects will be affected by these parameter estimates, our framework both establishes the underlying physics and likely provides qualitatively reliable trends. A limited comparison to a set of *ab initio* data obtained in the context of studies of Ref. 14 has been favorable, but showed both similarities and differences. It is remarkable that the symmetry of interactions in nanotubes imposes very definite requirements on the chirality dependence of the effects we discussed. A parametrization of our model using detailed *ab initio* calculations and experimental results for graphite and armchair or zigzag nanotubes will likely permit a further refinement of calculation outputs for nanotubes having any chirality.

ACKNOWLEDGMENTS

This work was supported by DARPA Grant No. MDA972-02-C-005 and the Robert A. Welch Foundation. We thank M. Kertesz for drawing our attention to the graphite data and for providing us with results of *ab initio* studies. We also thank S. Lee for his help with references.

[1] R. Saito, G. Dresselhaus, and M. S. Dresselhaus, *Physical Properties of Carbon Nanotubes* (Imperial College Press, London, 1998).

[2] *Carbon Nanotubes*: *Synthesis*, *Structure*, *Properties and Applications*, edited by M. S. Dresselhaus, G. Dresselhaus, and P. Avouris (Springer, Berlin, 2000).

[3] R.H. Baughman, A. Zakhidov, and W. deHeer, Science **297**, 787 (2002).

[4] J. Cumings and A. Zettl, Science **289**, 602 (2000).

[5] L. Forro, Science **289**, 560 (2000).

[6] R.H. Baughman *et al.* Science **284**, 1340 (1999).

[7] Y.N. Gartstein, A.A. Zakhidov, and R. Baughman, Phys. Rev. Lett. **89**, 045503 (2002).

[8] R. H. Baughman, A. Maiti, Y. N. Gartstein, R. Lakes, A. A. Zakhidov, and M. Kozlov (unpublished).

[9] Y. Miyamoto, A. Rubio, M.L. Cohen, and S.G. Louie, Phys. Rev. B **50**, 4976 (1994).

[10] L. Yang and J. Han, Phys. Rev. Lett. **85**, 154 (2000).

[11] Several combinations of elastic constants appear throughout the paper and we introduce their definitions here: $Z_{ab}=K_AK_B-K_{AB}^2$, $z_{ab}=K_A+K_B-2K_{AB}$, $z_a=2(K_B-K_{AB})/z_{ab}$, and $z_b=2(K_A-K_{AB})/z_{ab}$.

[12] J.P. Lu, Phys. Rev. Lett. **79**, 1297 (1997).

[13] D. Sánchez-Portal, E. Artacho, J.M. Soler, A. Rubio, and P. Ordejön, Phys. Rev. B **59**, 12 678 (1999).

[14] G. Sun, J. Kürti, M. Kertesz, and R. H. Baughman, J. Phys. Chem. B **107**, 6924 (2003).

[15] These considerations include symmetry requirements imposed by the following transformations: (1) nanotube axis inversion, $\phi\rightarrow\phi+\pi$; (2) reflection about the y axis accompanied by $\phi\rightarrow-\phi$; (3) rotation by $2\pi/3$. The results we use correspond to the first term of the Fourier expansion in the angular dependence.

[16] C.L. Kane and E.J. Mele, Phys. Rev. Lett. **78**, 1932 (1997).

[17] C. Chamon, Phys. Rev. B **62**, 2806 (2000).

[18] M. Verissimo-Alves, R.B. Capaz, B. Koiller, E. Artacho, and H. Chacham, Phys. Rev. Lett. **86**, 3372 (2000).

[19] M. Verissimo-Alves, B. Koiller, H. Chacham, and R.B. Capaz, Phys. Rev. B **67**, 161401 (2003).

[20] Note that here we correct the expression incorrectly shown in Ref. 7.

[21] M. Kertesz, in *Intercalated Graphites*, edited by M. Dresselhaus (Elsevier, Amsterdam, 1983), p. 141.

[22] S.Y. Hong and M. Kertesz, Phys. Rev. Lett. **64**, 3031 (1990).

[23] The curvature expansion contains only even powers of $1/R$ because this is the way all distances and scalar products of vectors modify when associated with atoms on a curved surface.

[24] The fact that $\delta\phi_l$ contains only odd powers of the curvature $1/R$ satisfies our notion that both these quantities are in fact associated with vectors/directions. Evidently, the torsion would occur in opposite directions when the parent horizontal sheet is wrapped upward vs downward to form a nanotube. On the other hand, the curvature-induced strain energy density (Refs. 1 and 25) and anisotropy of the elastic interactions have to be independent of the wrapping direction, and therefore are even functions of $1/R$.

[25] D.H. Robertson, D.W. Brenner, and J.W. Mintmire, Phys. Rev. B **45**, 12 592 (1992).

[26] E. Hernández, C. Goze, P. Bernier, and A. Rubio, Phys. Rev. Lett. **80**, 4502 (1998).